Smart Structures and Systems, *Vol. 27, No. 2 (2021) 209-226*
DOI: https://doi.org/10.12989/sss.2021.27.2.209

A new image-quality evaluating and enhancing methodology for bridge inspection using an unmanned aerial vehicle

Jin Hwan Lee [1a], Sungsik Yoon [2b], Byunghyun Kim [3c], Gi-Hun Gwon [1d], In-Ho Kim [4e] and Hyung-Jo Jung*[1]

[1] *Department of Civil and Environmental Engineering, Korea Advanced Institute of Science and Technology, 291 Daehak-ro, Yuseong-gu, Daejeon 34141, Republic of Korea*
[2] *Department of Civil and Environmental Engineering, University of Illinois at Urbana-Champaign, Urbana, IL 61801, USA*
[3] *Department of Civil Engineering, University of Seoul, Seoul 02504, Republic of Korea*
[4] *Department of Civil Engineering, Kunsan National University, 558 Daehak-ro, 54150, Republic of Korea*

(*Received October 9, 2020, Revised December 11, 2020, Accepted December 15, 2020*)

Abstract. This paper proposes a new methodology to address the image quality problem encountered as the use of an unmanned aerial vehicle (UAV) in the field of bridge inspection increased. When inspecting a bridge, the image obtained from the UAV was degraded by various interference factors such as vibration, wind, and motion of UAV. Image quality degradation such as blur, noise, and low-resolution is a major obstacle in utilizing bridge inspection technology based on UAV. In particular, in the field of bridge inspection where damages must be accurately and quickly detected based on data obtained from UAV, these quality issues weaken the advantage of using UAVs by requiring re-take of images through re-flighting. Therefore, in this study, image quality assessment (IQA) based on local blur map (LBM) and image quality enhancement (IQE) using the variational Dirichlet (VD) kernel estimation were proposed as a solution to address the quality issues. First, image data was collected by setting different camera parameters for each bridge member. Second, a blur map was generated through discrete wavelet transform (DWT) and a new quality metric to measure the degree of blurriness was proposed. Third, for low-quality images with a large degree of blurriness, the blind kernel estimation and blind image deconvolution were performed to enhance the quality of images. In the validation tests, the proposed quality metric was applied to material image sets of bridge pier and deck taken from UAV, and its results were compared with those of other quality metrics based on singular value decomposition (SVD), sum of gray-intensity variance (SGV) and high-frequency multiscale fusion and sort transform (HiFST) methods. It was validated that the proposed IQA metric showed better classification performance on UAV images for bridge inspection through comparison with the classification results by human perception. In addition, by performing IQE, on average, 26% of blur was reduced, and the images with enhanced quality showed better damage detection performance through the deep learning model (i.e., mask and region-based convolutional neural network).

Keywords: Unmanned Aerial Vehicle (UAV); bridge inspection; Image Quality Assessment (IQA); Image Quality Enhancement (IQE); damage detection

1. Introduction

The construction and maintenance of high-quality infrastructure, including bridges, dams, roads, and harbors, are essential factors for improving the quality of life in society. Among them, bridges are representative infrastructure and have been built simultaneously over the past few decades with the rapid economic development of modern society. In recent years, as bridges built intensively at that time are deteriorating, it causes various social problems such as collapse due to performance degradation. In general, the bridge inspection method requires a lot of experts and time, and additionally, various special equipment such as ladder truck, man-lift, or ground inspection vehicle. However, in the case of bridges built on the ocean or with complex structures, access to inspection is limited and, even if approached by well-trained inspectors, it is difficult to diagnose damage in detail. In addition, the existing methods are inefficient because they are time-consuming, labor-intensive, costly, confusing, and even unsafe for inspectors, and the inspection results include subjective interpretations (Jung *et al*. 2019).

In recent years, the use of an unmanned aerial vehicle (UAV) has grown in the field of bridge inspection and health monitoring. The growth of UAV-based inspection technology is due to their characteristics like versatility, flexibility, low cost, and minimized operational risk. (Gao *et al*. 2018) In particular, the use of a UAV for bridge inspection is suitable in that the bridge structure is generally complex and inaccessible, and it can be expected to have a great effect in that high-performance imaging devices can be freely mounted. Due to these advantages, numerous studies have recently been conducted related to bridge inspection using UAV (Hallerman and Morgenthal 2014,

*Corresponding author, Ph.D., Professor,
E-mail: hjung@kaist.ac.kr
[a] Ph.D. Student, E-mail: archi_tensai@kaist.ac.kr

ISSN: 1738-1584 (Print), 1738-1991 (Online)

Cunningham *et al*. 2015, Dorafshan *et al*. 2017, Seo *et al*. 2018, Tomiczek *et al*. 2018, Salaan *et al*. 2018, Jordan *et al*. 2018).

As shown in these various application cases, the performance and effectiveness of bridge inspection using vision images obtained from UAV are obvious, but there are still some important issues to be addressed prior to site application. Jung *et al*. (2019) emphasized the flight performance within the GPS denied area in the inspection phase, the occurrence of the missing field of view and deterioration of the image quality in the post-inspection phase, and the method of damage detection as major challenges prior to the actual application of UAV. Among them, a representative challenging issue in the post-inspection phase is the problem of image quality degradation due to internal factors (e.g., sensor performance, exposure times, motion modes, etc.) and external factors (e.g., rain, wind, movement, illumination, etc.), which lowers the accuracy of the damage detection, resulting in poor bridge assessment. Therefore, the selection and classification of high-quality images is the most important stage in the damage detection phase (Jeong *et al*. 2020). In particular, the most prominent type of quality degradation in images acquired from UAV systems is motion blurs that reduces the sharpness of the images. The degradation of sharpness adversely affects the damage detection phase, which is conducted based on edge extraction. Therefore, quality issues of image data must be addressed for accurate damage identification. Damage detection based on degraded images lead to inadequate results, which can restrict UAV's extended application (Kim *et al*. 2018, Kim and Cho 2019).

There are two ways to solve the quality problems mentioned above. The first is the use of image quality assessment (IQA) metrics to evaluate and select images that can be used for damage detection from a vast amount of image data sets. In general, if the damage within the bridge is clearly present and its location is known, the bridge inspection can be performed by taking a single image. However, if the existing inspection records for the target bridge are not secured or new damage appears, the bridge inspection should be performed by using multiple images of the entire bridge. In this case, numerous images are acquired through multiple flights, and it is very inefficient to classify and evaluate these data by the subjectivity of the inspector. To objectively and accurately assess the image quality, therefore, an objective method (i.e., IQA metric) that reflects the characteristics of the quality degradation caused by the motion blur of the UAV is required. Various conventional IQA metrics such as mean square error (MSE), peak signal-to-noise ratio (PSNR), or structural similarity (SSIM) evaluate the quality by comparing factors that affect quality based on distortion-free images. However, since the images obtained from UAV for bridge inspection cannot secure a distortion-free image, it is generally appropriate to apply the no-reference IQA metric to assess quality based on the characteristics of high-quality images.

Several researchers to identify high-quality images have applied many no reference (NR) IQA metric algorithms. Morgenthal and Hallermann (2014) and Sieberth *et al*. (2015) confirmed that blurs are generated through displacement between image frames caused by UAV's motion or wind effect, and emphasized that images degraded by blurs cause inaccuracies in damage detection. Duque *et al*. (2018) applied the combined entropy and sharpness algorithms for determining the high-quality images in the bridge inspection. They used the average entropy and sharpness values of the benchmark images to evaluate the quality through changes in the entropy and sharpness of each image obtained from the UAV. In addition, Jung *et al*. (2019) proposed a quality metric, noting that the quality deterioration due to the blur of the UAV image decreases the gradient of gray intensity between neighboring pixels.

Sieberth *et al*. (2016) proposed an automated image-filtering framework using saturation image edge difference (SIEDS) blur values. According to their proposed method, the blurred image included in the image set captured by UAV could be detected through a short processing time, and the detection speed and reliability were verified through two UAV datasets. However, while it was possible to filter blur images through relative image quality assessment using SIEDS value for independent image sets, there was no comparison for absolute image evaluation. Also, in the case of filtering for close range images, only the blur caused by linear camera displacement was considered, so it was not possible to determine the effect of various blur factors including dynamic motion that may occur in the close-range image set acquired based on UAV.

These processes of quality assessments may select images with high quality, but this may not be a fundamental solution. For example, if the quality of certain image frames essential for bridge inspection was degraded by motion blur or other reasons, additional work will be required, such as re-flight to re-acquire images of that area. At this time, if it is not possible to accurately know the shooting point of the image where the quality deterioration occurred, a more complex problem may be encountered. Therefore, numerous researchers have studied quality enhancement techniques for low-quality images to utilize the advantages of UAV-based bridge inspection technology in terms of time efficiency. Methods to improve the quality of images can be subdivided into a super resolution (SR) enhancement technique that improves low resolution and de-blur technique that reduces the degree of blurriness (Lei *et al*. 2018, Kim *et al*. 2016, Dong *et al*. 2016). The loss of image resolution is mainly caused by increasing the altitude of the UAV when capturing a wide geographical area, whereas a low- resolution problem rarely occurs when capturing a bridge from a distance of 2 to 3m. Rather, the deconvolution technique (deblurring) that recovers blurred images caused by UAV speed or unstable flight, wind, etc. is more important in the field of bridge inspection.

With the development of GPU and vision processing technology, the study of image de-blurring using deep learning was carried out (Wang *et al*. 2018, Burdziakowski 2020). In the field of civil engineering, Liu *et al*. (2020) proposed the deblur model based on the Generative Adversarial Network (GAN) for crack images. The

proposed model consisted of localized skip layers to demonstrate the correlation between the sharpened and the blurred crack image. That showed excellent de-blurring performance in feature restore and image sharpness, compared with various state-of-the-art deblur models. However, the performance of their method using GAN depends on the image characteristics and labeled training data. In addition, there is also a limitation that it takes a lot of time because of a lot of computation. These preliminary study cases are shown that the main issue facing UAV-based inspection technology is to obtain high-quality image data and that the quality of the data acquired initially is directly related to the final inspection results. In bridge inspection using UAV, it is necessary to judge the quality of the image through short processing time at the site and to enhance the quality or retake the image for low-quality imag8s.

In this paper, therefore, the proposed methodology is aimed to evaluate the quality of images acquired in bridge inspection using UAV and enhance the images with quality degradation such as blur, lack of exposure, etc. by using the de-blur algorithm. The image data set taken in the actual UAV was built and the quality was assessed using the blur operator and no-reference quality metric. In addition, image enhancement has been carried out using an optical flow-based kernel estimation method by classifying low-quality images. Based on the high-quality image data sets obtained through a series process of quality evaluation and enhancement, the deep learning technology and image processing technology were applied to detect the damage on the bridge. The reliability of quality assessment and enhancement effects were evaluated by comparing the detected damage information with the actual values.

The paper is organized as follows. Section 2 describes image quality metrics and quality enhancement techniques. The overall image processing process is covered in Section 3, and field experiment results and analysis using improved images are shown in Section 4. Finally, conclusions on the effects of applying image quality assessment and enhancement techniques are addressed in Section 5.

2. Theoretical background

The human eye can be a good classifier, but when inspecting large structures such as bridges, objective methods have the advantage of saving time and simplify the task. Objective IQA methods are classified into three categories: Full Reference (FR), Reduced Reference (RR), and No Reference (NR) or Blind Reference (BR). FR and RR require entire or partial images to be regarded as references. However, in the case of a special application such as a bridge inspection using a UAV, it is hardly possible to obtain the information regarding the reference image. Therefore, in this study, NR or BR IQA was applied among objective IQA methods to evaluate UAV images.

2.1 Quality assessment: The proposed method based on local blur map (LBM)

In this study, the method for evaluating image quality through blur map generation based on root mean square values (RMS) that emphasized faster and more perceptual contrast response was proposed. The local standard deviation of the image intensity of the image pixel $I(x,y)$ was used to generate the local blur map (LBM) of the input images. The LBM can be expressed as

$$LBM_{rms} = \sigma_{local}(x,y)^{\beta} \tag{1}$$

where $\sigma_{local}(x,y)$ is the local standard deviation of image intensities found in a neighborhood centered around a pixel at location (x,y). β denotes the parameter that increases the dynamic range of the local blur map and is expressed as an exponential of the local standard deviation of each pixel. The local standard deviation $\sigma_{local}(x,y)$ is computed using the intensity value $I(x,y)$ as

$$\sigma_{local}(x,y) = \frac{1}{2k+1}\sqrt{\sum_{i=-k}^{k}\sum_{j=-k}^{k}(I(x+i,y+j)-\mu_{local}(x,y))^2} \tag{2}$$

where $2k+1$ is the size of a local window in the vertical and horizontal directions. The term $\mu_{local}(x,y)$ is local window mean value that is computed as

$$\mu_{local}(x,y) = \frac{1}{2k+1}\sqrt{\sum_{i=-k}^{k}\sum_{j=-k}^{k}I(x+i,y+j)} \tag{3}$$

Next, the image array of LBM_{rms} is transformed from spatial to frequency domain using Discrete Wavelet Transformation (DWT). When blur occurs, features such as edges in the blurred image have discontinuities, and the image array of LBM_{rms} also shows discontinuities as well as more changes in the frequency domain. Given LBM_{rms} is decomposed into low frequency band made of DWT coefficient and three high frequency sub-bands containing horizontal, vertical and diagonal wavelet coefficients. In the final step, sorting the coefficients by ranking and weighting the wavelet coefficients is conducted.

2.2 Quality assessment: Conventional NR quality metrics

Among the NR IQA methods, commonly used are NIQE (Mittal *et al*. 2012b), BRISQUE (Mittal *et al*. 2012a), and SSEQ (Liu *et al*. 2014a). Mittal *et al*. (2012a) proposed NIQE based on the relationship between the statistical characteristics of the clean patch and sharpness and the similarity between the object image and the clean image meant the distance between qualities. Also, Mittal *et al*. 2012a proposed BRISQUE using the statistical characteristics of a natural image, which is Natural Scene Statistics (NSS), obtained by using Natural Image with Mean Subtraction and Contrast Normalization (MSCN). They noted that when distortion occurs in the natural image, the statistical characteristics of the image pixels are also distorted, and they specified the feature and information of

the Generalized Gaussian Distribution (GGD) consistent with the MSCN histogram of the distorted image. After deriving the features, it is training the Support Vector Machine (SVM) using the features and labels to predict the quality of the image. The NR IQA methods (i.e., NIQE, BRISQUE, and SSEQ) as mentioned above assessed the image with a high score to a "distortion-free" image, that is, a natural image. The distortion is determined by comprehensively considering features that appeared inside the image such as noise, blur, and exposure.

However, in the case of UAV images, since blurriness is the main reason of quality degradation, there are IQA methods of the blurred image by calculating the degree of the blurriness that occurs mainly inside the image. Jung *et al*. (2019) proposed the quality metric based on the sum of gray-intensity variance (SGV). This method was established based on the fact that when blurs occurred, the sharpness of the image decreased, and the gradient value of the grays-intensity between neighboring pixels also decreased. On the other hand, when blur hardly occurred, since the sharpness value increased relatively, the gradient of gray-intensity between neighborhood pixels increased. Liu *et al*. (2014b) proposed a blur measure operator that can detect blurred images without kernel estimation using the singular value decomposition (SVD). This method evaluates the image based on the relationship between the change in the singular value and the degree of blurriness. To measure the blur, a singular value is obtained in units of pixels or image neighborhood windows, and high-frequency details of the eigen-image are discarded on a small scale through a convolution operator. Accordingly, detailed information of the image decreases, and the weight of the unique image at this time increases. As a result, blurred images usually have a much higher weight than clear images. Golestaneh and Karam (2017) conducted the high-frequency discrete cosine transform (HiFST) to obtain the DCT coefficients of gradient magnitudes by using neighboring windows of varying sizes around the center pixel, sorting, grouping them into multiple layers. The DCT coefficient can represent different frequencies, and it includes information related to image structure, energy, and blurriness.

For the relative comparison between the proposed quality metric and other quality metrics, the log values of diagonal wavelet coefficients were used and the conventional blur map $BM(x,y)$ was generated by using blur operator B.

$$BM(x,y) = B(I(x,y)) \tag{4}$$

where $I(x,y)$ is a blurred input image for which the amount of blurriness is to be computed at each pixel location. The blur map is normalized linearly so that $BM(x,y) \in [0,1]$. The normalized blur map can be expressed as

$$\widehat{BM}(x,y)) = 1 - \frac{BM(x,y) - min(BM)}{max(BM) - min(BM)} \tag{5}$$

where $max(BM)$ and $min(BM)$ mean the value of the maximum and minimum degree of blurriness in the blur map.

2.3 Quality enhancement: The algorithm of blind image deconvolution

In general, the process of motion blurs in UAV images is modeled as

$$BI = k * L + N \tag{6}$$

where BI is blurred image, k denotes the motion-blur kernel, and L is the latent image. N denots the noise and $*$ is a convolution operation. Since blurred images of UAV do not have a reference image, deblurring is an ill-posed problem with unknown numbers more than observed data. A successful approach is alternating optimization of latent image L and blur kernel k in an iterative processes. The standard energy function of image deblurring (Cho and Lee 2009) can be expressed as

$$f(\mathrm{L},\mathrm{K}) = |B - L * k|^2 + q(L) + r(K) \tag{7}$$

where (L) , $r(K)$ is regulization terms or priors for L, K. In general, the image deblurring process is an iterative process of performing latent image estimation and kernel estimation based on the estimated latent image. However, it is difficult to restore an image that is blurred by an ununiformed blur kernel such as motion blur in UAV by the conventional image deconvolution method. In order to restore a blurred UAV image, deconvolution with precisely estimated blind blur kernel by reflecting the motion of the UAV is essential. Therefore, in this study, the method of variational Dirichlet (VD) blur kernel estimation proposed by Zhou *et al*. (2015) was applied. They addressed the blur problem by replacing two optimization problems as

$$x^{k+1} = \operatorname{argmin} \sum_i \frac{1}{2} \|\nabla_i H^k x - y\|_2^2 + \lambda_x R_x(x), \tag{8}$$

$$h^{k+1} = \operatorname{argmin} \sum_i \frac{1}{2} \|\nabla_i X^{k+1} h - \nabla_i y\|_2^2 + \frac{\lambda_h}{2} R_h(h), \quad \text{subject to} \quad \mathrm{h} \geq 0, \ \sum_j h(j) = 1 \tag{9}$$

where $\nabla_i X^{k+1}$ is the matrix formed by the gradient of the image x^{k+1} utilizing the i-th filter, k denotes iteration index , H^k is the convolution matrix formed by the estimated impulse response of the blur at the k-th iteration step h^k and R_h is the regularization function. The parameters λ_x , λ_h are crucial to get better kernel estimation results and λ_h help to adjust the smoothness of the kernel and avoid the delta kernel. As the value of λ_h increases, the kernel becomes wider and shows more noise, which is generally proportional to the image size and noise level. The results of parameter studies of λ_h and λ_x can be confirmed by referring to previous paper, and λ_x = 0.0002 and λ_h = 0.01 values were used in this study.

3. The proposed approach

The typical procedure of the bridge inspection using

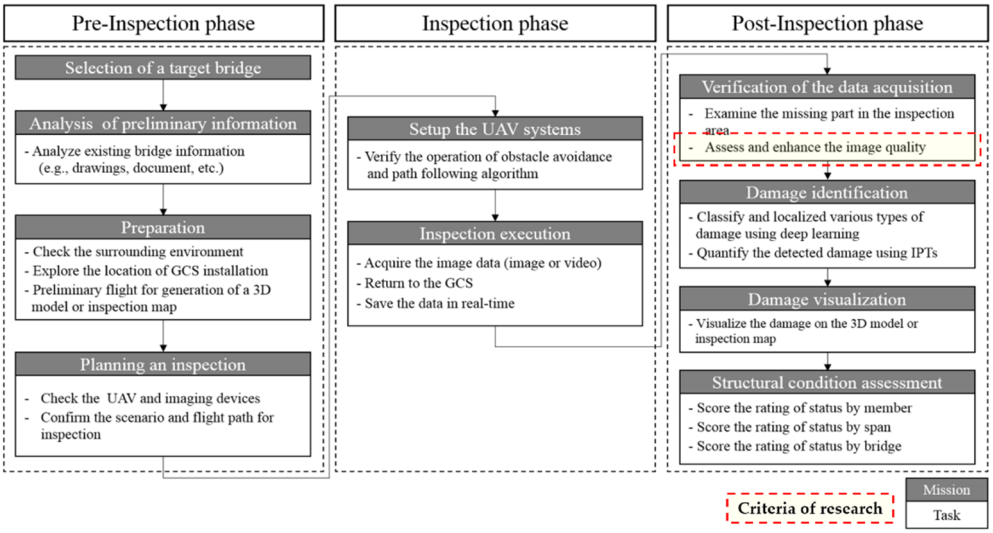

Fig. 1 Typical procedure of bridge inspection using UAV proposed by Jung *et al*. (2019)

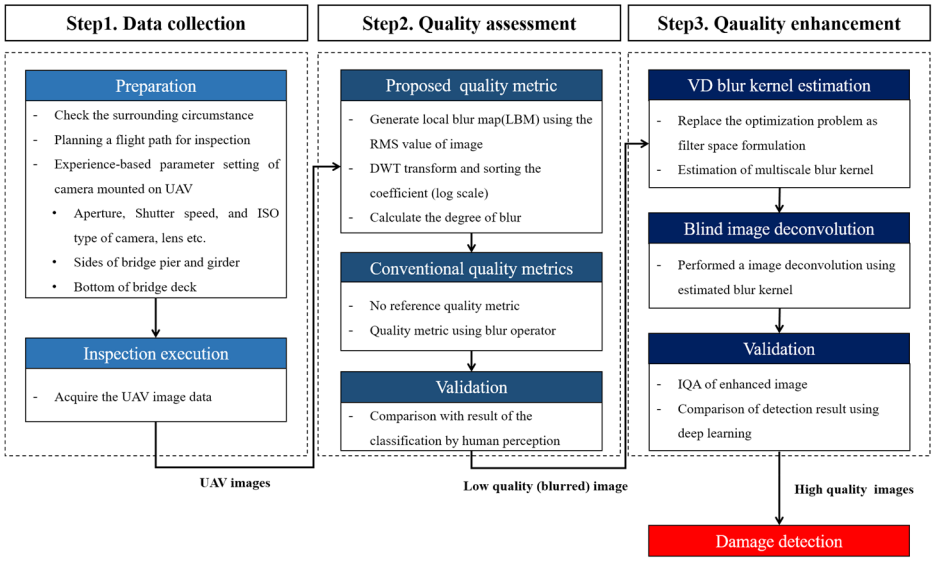

Fig. 2 The overall flowchart of the proposed research

UAV proposed by Jung *et al*. (2019) consists of three phases as shown in Fig. 1. This study focused on the verification of data acquisition in the post-inspection phase, and this mission consists of two sub-missions. One sub-mission is to detect the missing area among the inspection areas, and this problem can be addressed through an algorithm based on UAV metadata and camera attitude information proposed by Yoon *et al*. (2020). The remaining sub-mission of the verification process is related to an objective assessment of image quality and methods of enhancing the quality of degraded UAV image.

In this study, to address the quality issue in the bridge inspection process using UAV mentioned in chapter 1, a methodology consisting of three steps was proposed as shown in Fig. 2. In Step 1, parameter values of a camera related to illuminance that vary depending on the bridge member were discussed, and data collection was performed by applying them. In Step 2, a new quality metric for IQA was proposed, and performance validation was performed through comparative analysis with the results of existing methods. The process of validation was conducted by comparing the result of applying each quality metric to the material image set and the result classified by the perspective of the inspector in advance. The different thresholds were applied for each metric to the result of image quality quantification, and classification into high-quality and low-quality images was performed. In Step 3, IQE was performed on low-quality images. The method of IQE was divided into a blur kernel estimation and a blind image deconvolution using a kernel. The details of each step were described below, and validation tests based on this proposed methodology was conducted and described in Section 4.

3.1 Step1: Data collection process

Generally, images with good quality mean well-exposed images by adjusting the camera's internal parameters such

as aperture, shutter speed, and ISO sensitivity. However, due to the nature of the UAV platform, it is difficult to secure a good quality image due to frequent interference from external factors (i.e., velocity of UAV, wind speed, shadow, etc.). Nevertheless, based on the experience gained through many flying for inspection in various environments, the method of setting the parameter of camera and flight guides that can minimize blur and satisfy good exposure conditions was proposed. When inspecting an actual bridge using a UAV, the images obtained according to the values of the internal parameters were various results as shown in Fig. 3. ISO sensitivity was defined as sensor gain, and higher values increase the brightness of the image, but the quality of the image decreases due to noise. The shutter speed and size of the aperture determined the amount of light exposed to the sensor during image capture. Longer exposures to light (lower shutter speed) can cause more motion blur, and smaller aperture values result in greater distortion around the image, resulting in poor quality (O'Connor *et al*. 2017). Assuming a UAV flying automatically through a given path, when flight under a bridge with relatively low light, the ISO value should be raised and the shutter speed was set faster to minimize the occurrence of noise and blur. In the case of outside piers and girders with adequate exposure, the ISO value should be minimized and the aperture size should be increased to minimize distortion occurring outside the image frame.

The examples of UAV images in bridge inspection according to the various camera parameter settings have been shown in Fig. 3. Here, Figs. 3(c), (d) and (f) were well-exposed images, Fig. 3(a) was over-exposed, and Figs. 3(b) and (e) were a low-exposed image. In particular, Fig. 3(a) was the bridge's pier section where sunlight was reflected, resulting in over-exposure due to the slow shutter speed setting. In addition, Fig. 3(e) was the deck floor of the bridge with less sunlight, which was intended to secure well exposure by increasing the ISO value, but due to the incorrect shutter speed setting, there was a lack of exposure. On the other hand, image Fig. 3(b) lowered the shutter speed so that sufficient light could enter the sensor to secure exposure, while Figs. 3(c) and (d) were able to obtain images with less distortion of the surrounding through the setting of fast shutter speed and aperture opening control. Fig. 3(f) is an example of securing sufficient exposure by lowering the shutter speed because the area where the amount of illumination entering the sensor is small compared to Fig. 3(e). Although the parameter values shown in Fig. 3 are not fixed values that apply to all situations, it can be seen that the camera parameter setting considering the ambient conditions when inspecting a bridge using UAV has a great influence on the image quality. Table 3 shows the internal parameter settings of the camera used in this study.

3.2 Step2: *Image quality assessment* (*IQA*)

In step 2, image quality assessment based on DWT coefficients is performed, and the performance of the

(a)1/50sec, f/5.6 ISO 100 (b) 1/250sec, f/4, ISO 400 (c) 1/800sec, f/4.5, ISO 100

(d) 1/640sec, f/3.5, ISO 320 (e) 1/1250 sec, f/2.8, ISO 320 (f) 1/200 sec, f/2.8, ISO 320

Fig. 3 Examples of obtaining image for bridge inspection using UAV

Table 1 Camera parameter setting according to the amount of illumination used in this study

Sides of bridge pier and girder (bright area)		Bottom of bridge deck (shadow area)	
ISO sensitivity	100~320	ISO sensitivity	≥320
Aperture size	f/4.5 ~ f/5.6	Aperture size	f/3.5
Shutter speed	1/250 ~ 1/800sec	Shutter speed	1/100 ~ 1/250sec

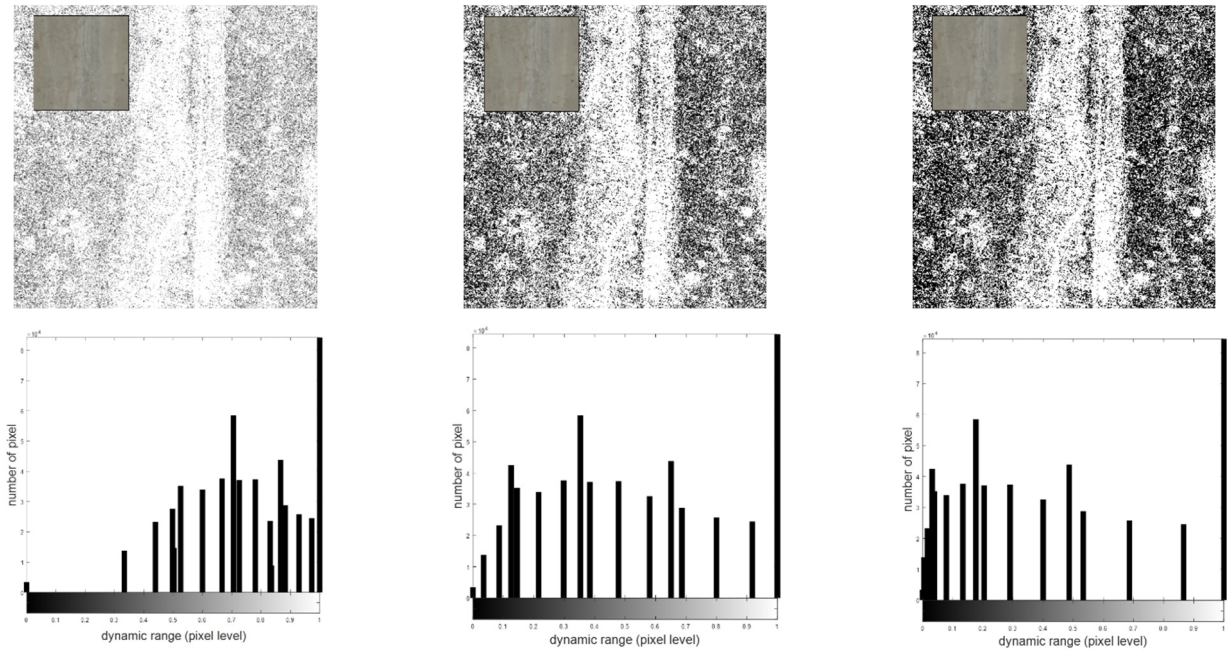

(a) $\beta = 0.5$ (b) $\beta = 3.5$ (c) $\beta = 5.5$

Fig. 4 Changes in dynamic range of input image as exponential coefficient increases

proposed method is confirmed by comparing with the results of applying conventional metrics. The purpose of performing IQA is to secure images to be used for damage detection by quantifying the quality of raw images obtained from UAVs and to select low-quality images for image enhancement. As shown in Fig. 2, image quality evaluation consists of three steps, and firstly, the input image in RGB scale is converted to a gray scale image. Then, the initial local blur map is generated using the local standard deviation of image intensity and the local window mean value as shown in Fig. 4. The exponential coefficient shown in Eq. (1) increases the dynamic range of the input image converted to gray scale. Fig. 4 shows the change of the dynamic range as the exponential coefficient increases. When the value of β increases from 0 to 4, the dynamic range increases as shown in Figs. 4(a) and (b). However, when it is increased to 4 or more, the pixel change is performed toward the lower brightness level, and the dynamic range tends to narrow as shown in Fig. 4(c). Therefore, in this study, the exponential coefficient value for generating local blur map was set to 3.5.

Next, DWT is performed to convert the generated initial LBM into the frequency domain. Fig. 5 is the result of decomposing the converted LBM into a low-frequency band and a high-frequency sub-band. Finally, the wavelet coefficient of the high frequency is weighted and converted into a log scale value to score the degree of blurriness in the image. Fig. 5 shows the local blur maps using input images with various blur conditions. As degree of blurriness increases, the contrast of the local blur map increases. Increasing the contrast of the local blur map means that the rate of occurrence and distribution of the blur is higher. The scores of image quality are calculated by the log scale value using weighted wavelet coefficient value of each local blur map.

In order to compare with the proposed method, IQA is performed using other conventional quality metrics. The NR quality metrics (i.e., NIQE, BRISQUE, and SSEQ) were used to comprehensively evaluate image quality. These algorithms were implemented through open sources (MATLAB codes) released by the Laboratory of LIVE at the University of Texas at Austin. In addition, methods of SVD and HiFST were used to quantify the quality based on the degree of blurriness, all processes of IQA were performed on a desktop having Intel Core i7 5930K with Nvidia GeForce GTX1070 graphic card and 48GB RAM using MATLAB 2017a.

Fig. 6 shows an equation for calculating blurriness through each quality metric and the process of classifying image quality by applying a threshold with a normalized image quality score. The metric as shown in Fig. 6(a) that utilizes the variance of neighbor pixel-to-neighbor gray intensity notes the nature of blurs occurring resulting in a reduction in sharpness. However, if shadows often occur in the image as shown in Fig. 3(b), or Fig. 3(e), the results of the blur detection are inaccurate. Other quality metrics as shown in Fig. 6(b) note that the singular value decomposition process is similar to the image blurring that keeps structure at large scale, and discards the detail of image at small scales (Su *et al*. 2011). The other metric as shown in Fig. 6(c) notes that the blur area has a lower DCT coefficient value than the sharp area, and the degree of blur is determined through multi-scale fusion, sorting, and normalizing processes using high-frequency DCT coefficient value. As described above, a comparative analysis was performed between the results of applying three quality metrics operating on different principles.

In order to classify into two groups using the quality score calculated through the IQA process, it is essential to apply an appropriate threshold value. Among previous

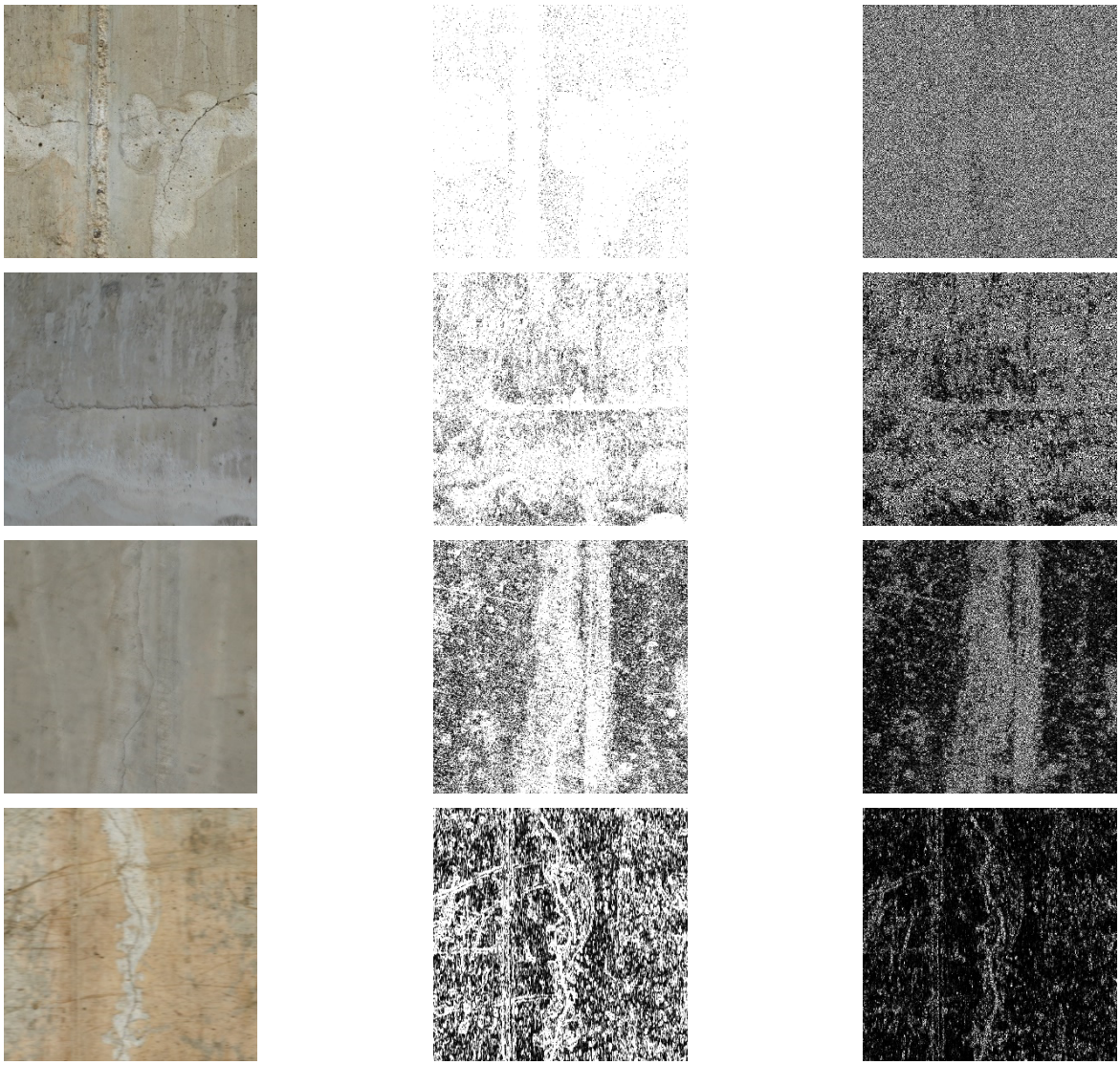

(a) Orginal input (b) LBM$_{inital}$ (c) LBM$_{final}$

Fig. 5 The results of the proposed method using LBM

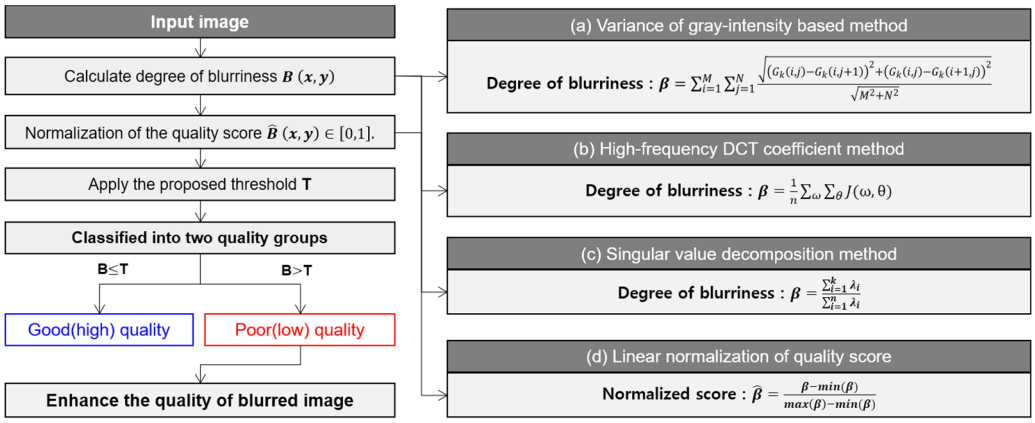

Fig. 6 The procedures of compared method using SVD, HiFST, and SGV

studies related to this, Jung *et al*. (2019) performed SGV based quality assessment, and quality classification was performed by setting criteria of $\pm 2\sigma$ from the mean value of the quality score in local image set. However, in this case, when the mean value of quality score of the local image set is generally low, the threshold value may not be

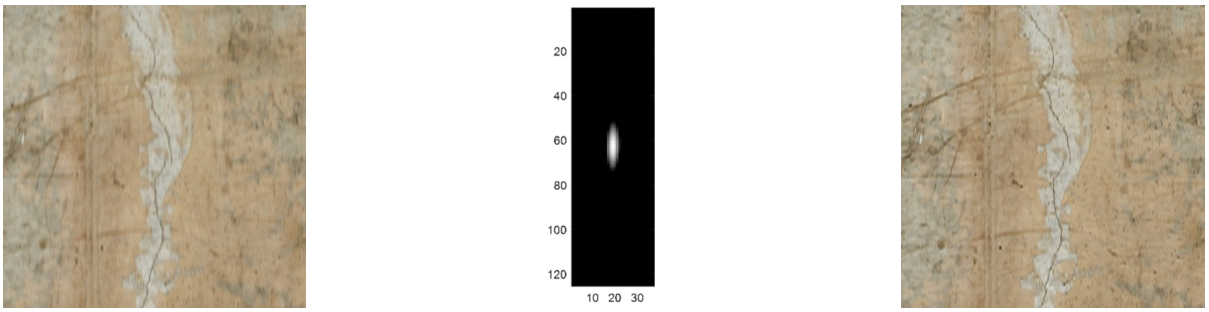

(a) Blurred image (b) Estimated kernel (c) Deblurred image

Fig. 7 Blind image deconvolution based on VD kernel estimation method

(a) Target bridge (b) UAV system

Fig. 8 Field application of bridge inspection using UAV

appropriate. Therefore, in this paper, linear normalization of the quality score of each image was performed using a set of 2,700 UAV images captured in various environments. By setting $m - 2\sigma$ as the threshold value using the mean value and standard deviation of the normalized score in the UAV image data set, the disadvantages of the threshold using the local image set mentioned above were compensated.

3.3 Step 3: Image quality enhancement (IQE)

In step 3, the algorithm of image enhancement that performs blind image deconvolution by estimating the blur kernel using the variational Dirichlet (VD) method proposed by Zhou *et al*. (2015) is applied to the UAV image. This method is based on the image prior to non-dimensional Gaussianity measures to enforce sparsity and an undermined boundary condition to reduce the boundary artifacts. Since the shape of blurriness occurring in UAV images is not constant, non-uniform kernel estimation using Dirichlet distribution was used to approximate the posterior distribution of the blur. Here, the parameter value λ_x is set to 0.0002 as the default value and 1000 iterations for estimating blur kernel. The input image containing concrete crack shown in Fig. 7(a) was a cropped image (1000 by 1000 pixel) from the original image captured by UAV, and artificially generated blur by applying 2D-Gaussian filtering within the cropped image. When the magnitude of sigma is $\sigma_x = 2\sigma$ and $\sigma_y = 8\sigma$, the blur kernel estimated through the VD method was shown in Fig. 7(b).

4. Validation: application to real UAV images

4.1 Imaging device and UAV system for acquiring material images

When inspecting a bridge, it was common to select cameras and UAV differently depending on the purpose and target structure. However, when using a commercial UAV, there are disadvantages in that flight time and performance are limited, and the range of camera selection is narrow. For example, Salaan *et al*. (2018) used a UAV equipped with a passive rotating spherical shell structure to detect surface cracks at a distance of 0.5 m, and Myeong and Myung (2018) used a type of wall-climbing UAV for performing a micro inspection. The performances of the UAV used in this study were a maximum takeoff weight of 19 kg, an average flight time of 30 minutes, and a quadrotor type designed to be equipped with a high-performance imaging device (i.e., DSLR camera). In addition, the gimbal attached to this UAV not only serves to fix the imaging device but also helps to reduce vibrations caused by the wind. Also, the gimbal was effective for photographing various members of the bridge as it can switch the camera in the direction of roll and pitch ($\pm 90°, \pm 90°$). The imaging device used in this study is a high-resolution DSLR camera (i.e., Sony alpha9) capable of capturing single images with 24 million pixels (6000 × 4000), and a lens with fast autofocus and optical image stabilization functions was used (i.e., ZEISS Batis 85 mm f/1.8) as shown in Fig. 8(b).

The target bridge was selected as the D Bridge in

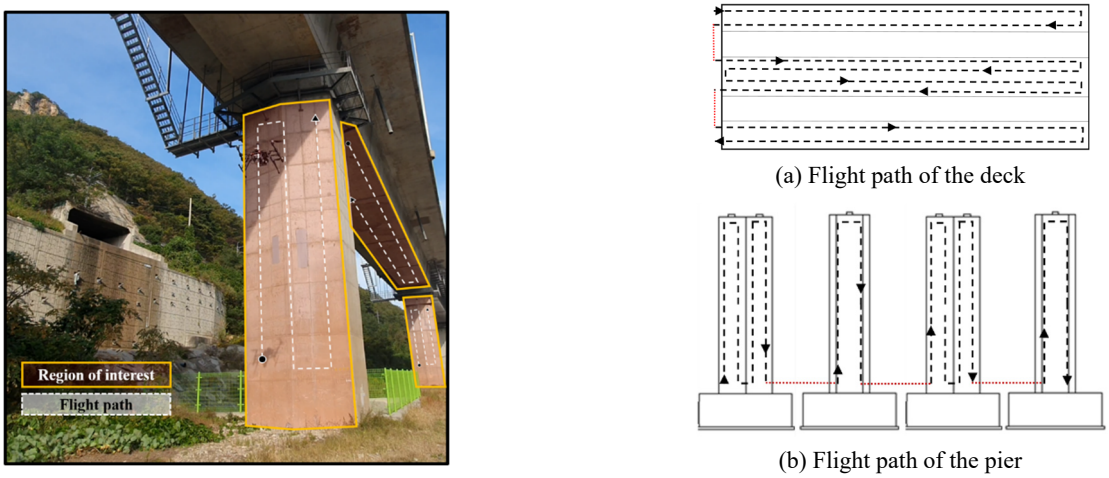

(a) Flight path of the deck

(b) Flight path of the pier

Fig. 9 Flight path of each bridge member

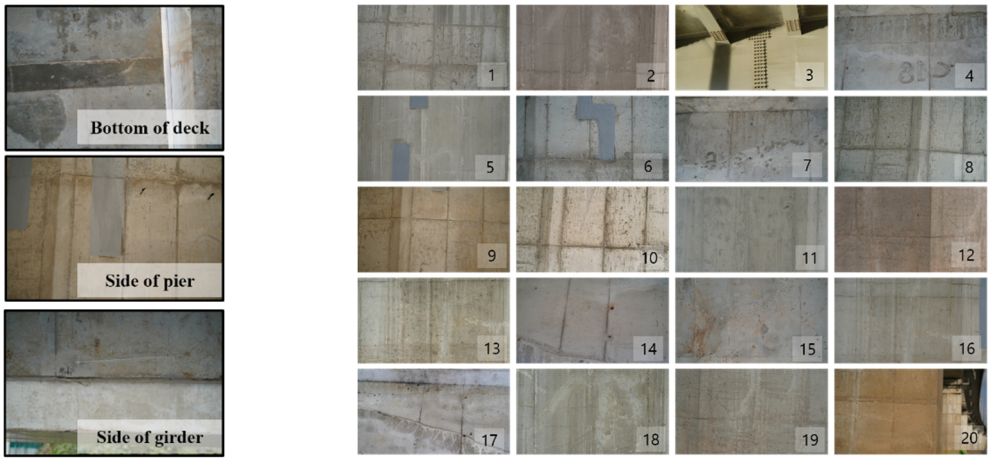

Fig. 10 Material image sets for validation test

Gangwon province, South Korea, as shown in Fig. 8(a). This bridge consists of 10 steel boxes and 10 PSC box girders, and the bridge piers, decks, and sides were inspected. The inspection path for each member of the bridge is shown in Fig. 9, and the continuous acquisition of images was performed while maintaining the operating distance of about 2 m to 4 m. Among the numerous images (about 2,700 images) obtained from UAV for the validation test, 20 images were selected and composed as a material set. Material images consisted of clear images that can be perceived by humans and images with various types of quality degradation such as blur, defocusing, and noise. The flight path for each member to photograph the material data used for the validation test was shown in Fig. 9, and the acquired images were shown in Fig. 10.

The target bridge was selected as the D Bridge in Gangwon province, South Korea, as shown in Fig. 8(a). This bridge consists of 10 steel boxes and 10 PSC box girders, and the bridge piers, decks, and sides were inspected. The inspection path for each member of the bridge is shown in Fig. 9, and the continuous acquisition of images was performed while maintaining the operating distance of about 2m to 4m. Among the numerous images (about 2,700 images) obtained from UAV for the validation test, 20 images were selected and composed as a material set. Material images consisted of clear images that can be perceived by humans and images with various types of quality degradation such as blur, defocusing, and noise. The flight path for each member to photograph the material data used for the validation test was shown in Fig. 9, and the acquired images were shown in Fig. 10.

4.2 Material image sets of bridge inspection using UAV

These UAV images were taken with different camera internal parameters and were compressed in JPEG format. The resolution of the images follows two types of digital format 10 MP (3936 × 2624), 24MP (6000 × 4000). In order to perform the process of the quality assessment and enhancement using UAV images taken in various environments, several inspection flights were performed, and images of the bottom of the bridge deck, the side of the pier, and the side of the girder were taken as shown in Fig. 10.

Before applying the proposed quality metric based on blur operator, classification by the inspector's perspective and assessment using the NR quality metric were

(a) Sharpened images (#6, #13)

(b) Blurred images (#14, #15)

Fig. 11 Examples of the classified to high and low quality

Table 2 The results of image classification based on subjective criteria of the inspector

Quality metric	Categorized material images in quality group	
	High quality	Low quality
Subjective classification	#1, #3, #6, #8, #9, #10, #13, #18, #20 #3 (sharpened, shadow area)	#2, #4, #5, #7, **#11**, #12, **#14**, #15, #16, #17, #19 #12 (ambiguous) #11 (larger degree of blurriness) #14 (lager degree of burriness)

performed. The purpose of the preliminary image assessment was to confirm whether the NR quality metrics commonly used for natural image quality evaluation, such as NIQE, BRISQUE, and SSEQ, were suitable to be applied to UAV imagery. In addition, the classification result was objectively determined by comparing the result of image classification performed by the subject of the inspector and the result of image quality classification based on the quality metric proposed in this study.

Here, classification by the perspective of the inspector means classifying images by the degree of perception of blur in the image. From the 20 material images, 11 images contained blur, and especially two images (#11, #14) were considered to have a larger degree of blur. The result of classifying the images into two classes was shown in Table 2.

Next, the material image set of UAV images was assessed by using three quality metrics, which were used for quality assessment of the natural image. As a result of evaluating the image quality using the BIRSQUE metric, it was confirmed that the quality of the 2 images (#2, #12) was the lowest, and the 6 images (#5, #11, #16, #17, #18 and #19) were lower than the average score as shown in Fig. 12(a). As a result of classification using the NIQE metric, 10 images (#2, #3, #5, #11, #13, #14, #16, #17, #18 and #19) could be distinguished as low-quality images. In addition, it was confirmed that the quality of the three images (#2, #12, and #18) has relatively lower scores through image quality assessment using the SSEQ metric. Although, two images (#3, #18) were considered as the sharpened image from the perspective of an inspector, an error of classification as a low-quality image occurred. In short, BRISQUE, NIQE, and SSEQ metrics were the most representative NR quality metrics for evaluating image quality, but when compared to the subjective classification results, they were insufficient in part to properly measure and evaluate the degree of blur in the image.

4.3 Comparison and analysis of IQA results using various blur operators

The results of three quality metrics based on the degree of blur through pixel-wise processing, not the characteristics of natural images were shown in Fig. 13. The threshold values of each quality metric were $T_{\text{svd}} = 0.786$, $T_{\text{HiFST}} = 0.7096$, $T_{\text{Proposed}} = 0.7112$ and $T_{\text{SVG}} = 0.6884$, and the classification results were shown in Table 4. The scores of the material images obtained through three metrics

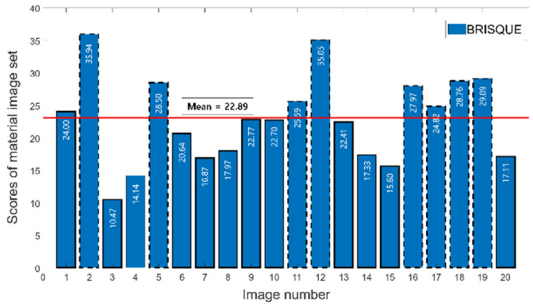

(a) BRISQUE (blue)

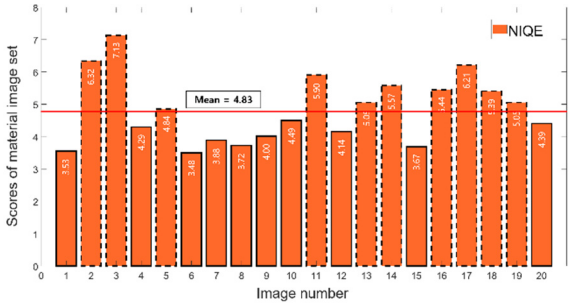

(b) NIQE (orange)

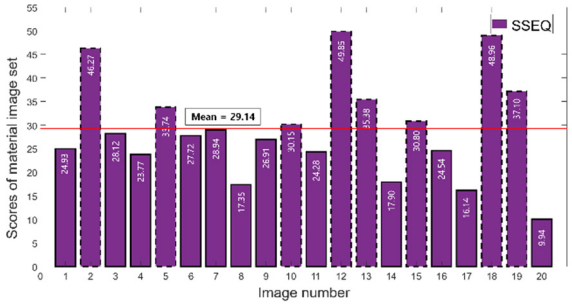

(c) SSEQ (purple)

Fig. 12 Results of applying each NR quality metric to 20 material images

Table 3 The results of applying quality evaluation criteria based on natural image characteristics

Quality metric		Categorized material images in quality group	
		High quality	Low quality
NR quality metric	BRISQUE	#3, #4, #6, #7, #8, #9, #10, #13, #14, #15, #20	#2, #5, #11, #12, #16, #17, #18, #19
	NIQE	#1, #4, #6, #7, #8, #9, #10, #12, #15, #20	#2, #3, #5, #11, #13, #14, #16, #17, #18, #19
	SSEQ	#1, #3, #4, #6, #7, #8, #9, #11, #14, #16, #17, #20	#2, #5, #10, #12, #13, #15, #18, #19

(i.e., SVD, HiFST, and SGV) were normalized to the [0, 1] for relatively easy comparison. Since the quality scores were obtained by the normalized degree of blurriness by using Eq. (5) that was calculated by each blur operator, the higher the score, the better the quality.

The image quality scores measured through blur map generation based on the blur operators (SVD, HiFST, SGV, and proposed) were shown in Figs. 13 and 14. By applying the threshold value for each metric, the image quality was classified into two classes. As a result of quality classification using the SVD method shown in Fig. 13(a), a total of 11 images were lower than the threshold value ($T_{\mathrm{svd}} = 0.786$) and image #19 was evaluated as the lowest quality. As a result of quality classification using the HiFST method shown in Fig. 13(b), a total of 11 images were classified as low quality, of which image #12 was evaluated as the lowest quality.

As a result of SGV-based quality evaluation shown in Fig. 14(a), a total of 7 images were classified as low quality, of which image #20 was evaluated as the lowest quality. As

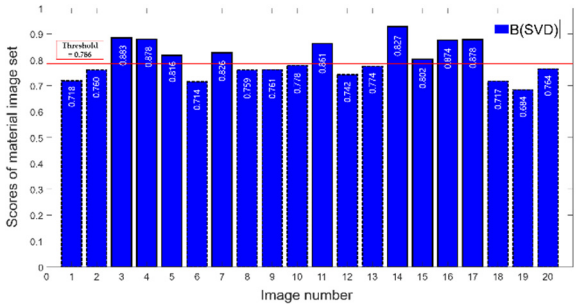

(a) SVD (blue)

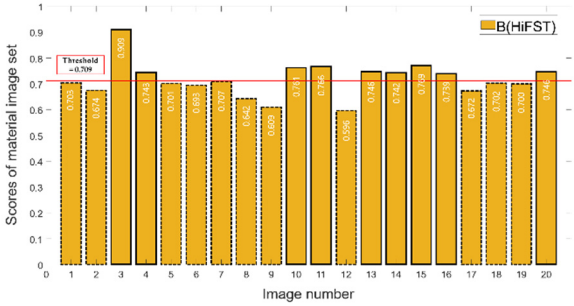

(b) HiFST (yellow)

Fig. 13 The Results of applying each quality metric based on blur operator

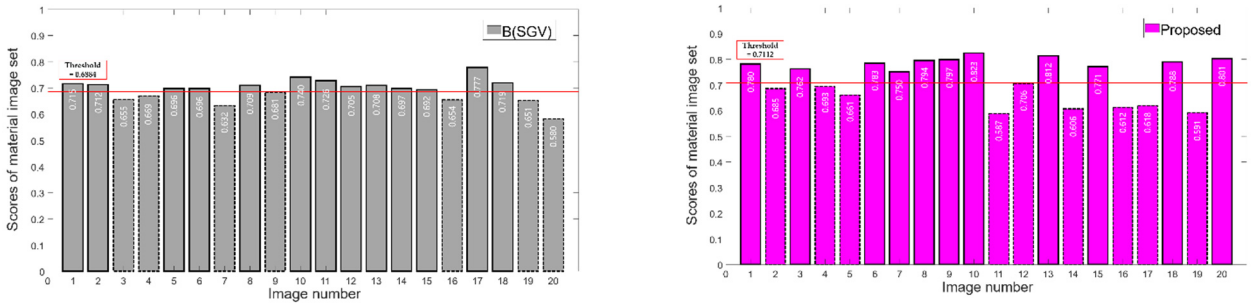

(a) SGV (gray) (b) The proposed method (magenta)

Fig. 14 The Results of applying each quality metric based on blur operator

Table 4 Results of applying quality evaluation criteria based on blur image characteristics

Quality metric		Categorized material images in quality group	
		High quality	Low quality
Blur operator based quality metric	SVD	#3, #4, #5, #7, #11, #14, #15, #16, #17	#1, #2, #6, #8, #9, #10, #12, #13, #18, #19, #20
	HiFST	#3, #4, #10, #11, #13, #14, #15, #16, #20	#1, #2, #5, #6, #7, #8, #9, #12, #17, #18, #19
	SGV	#1, #2, #5, #6, #8, #10, #11, #12, #13, #14, #15, #17, #18	#3, #4, #7, #9, #16, #19, #20
	Proposed method	#1, #3, #6, #7, #8, #9, #10, #13, #15, #18, #20	#2, #4, #5, #11, #12, #14, #16, #17, #19

a result of applying the proposed method in this study shown in Fig. 14(b), a total of 9 images were evaluated as low quality, and image #11 was evaluated as the lowest quality. The quality metric proposed in this study showed the most similar results to subjective classification results of the inspectors shown in Table 4, and the quality classification results of the material image set except for image #7 were very similar. The image quality metric proposed in this study has the advantage that it can be used not only for relative comparison between images but also for absolute comparison through normalized scores.

4.4 Analysis of IQE results and validation using deep learning model

In the previous section, low-quality images having a quality score lower than the threshold were classified. Based on the results of applying the proposed quality metric, a total of 6 images (4, #5, #11, #14, #16, and #19) were selected as target images for quality improvement. The size of the blurred patch was 1000 by 1000 pixels, and the blurred patch of the damaged part in the ROI as shown in Fig. 11(b) was cropped and used as an input image. The estimated kernel size as shown in Fig. 15(b) was 125 by 37 pixel or 37 by 125 pixel and the results of blind deconvolution were as shown in Fig. 15(c). The parameter λ_x is set to 0.0002 as the default value and 1000 iterations for estimating the blur kernel. This process was performed on a desktop having Intel Core i7 5930K with Nvidia GeForce GTX1070 graphic card and 48 GB RAM using MATLAB 2017a.

The shape and size of the blur kernel shown in Fig. 15(b) correlated with the degree of blurriness, and through this, the main cause of blur can be estimated. Since the blur kernels of three images (#4, #5, and #11) were not large in vertical and horizontal directions, it was confirmed that the blur of the image was caused by the vibration of the camera rather than the motion of the UAV. On the other hand, since the blur kernels of the three images (#14, #16, and #19) were non-uniform and had a size in the vertical or horizontal direction, it can be seen that the motion of UAV was the main cause of blur. The deconvolution process was performed through the estimated blur kernel, and the results are shown in Fig. 15(c). When compared with the input image, the resulting image is clearly distinguished from damage such as cracks and leaks, which is expected to reduce the probability of false-alarm occurring in the damage detection phase.

To confirm how much the quality of the enhanced image was improved quantitatively, re-evaluation was performed using the previously applied quality metric. As a result of performing a quality assessment with 6 enhanced images, the scores improved by 20.65%, 26.39%, 27.68%, 30.87%, 40.11%, and 13.89% respectively. Through an average of 26% improvement in the score as shown in Fig. 16, quality scores above the threshold value were secured for all images, which was a level considered as data that could be used in the damage detection phase.

In addition, the damage detection technology through deep learning was applied to see how the image quality improvement affects damage detection. The deep learning model used for damage detection was the mask and region-based convolutional neural network (Mask R-CNN) model. In this study, the Mask R-CNN model using the backbone ResNext-101 (Xie *et al*. 2017) was trained on a dataset consisting of 1276 cracks, efflorescence, and rebar exposure images.

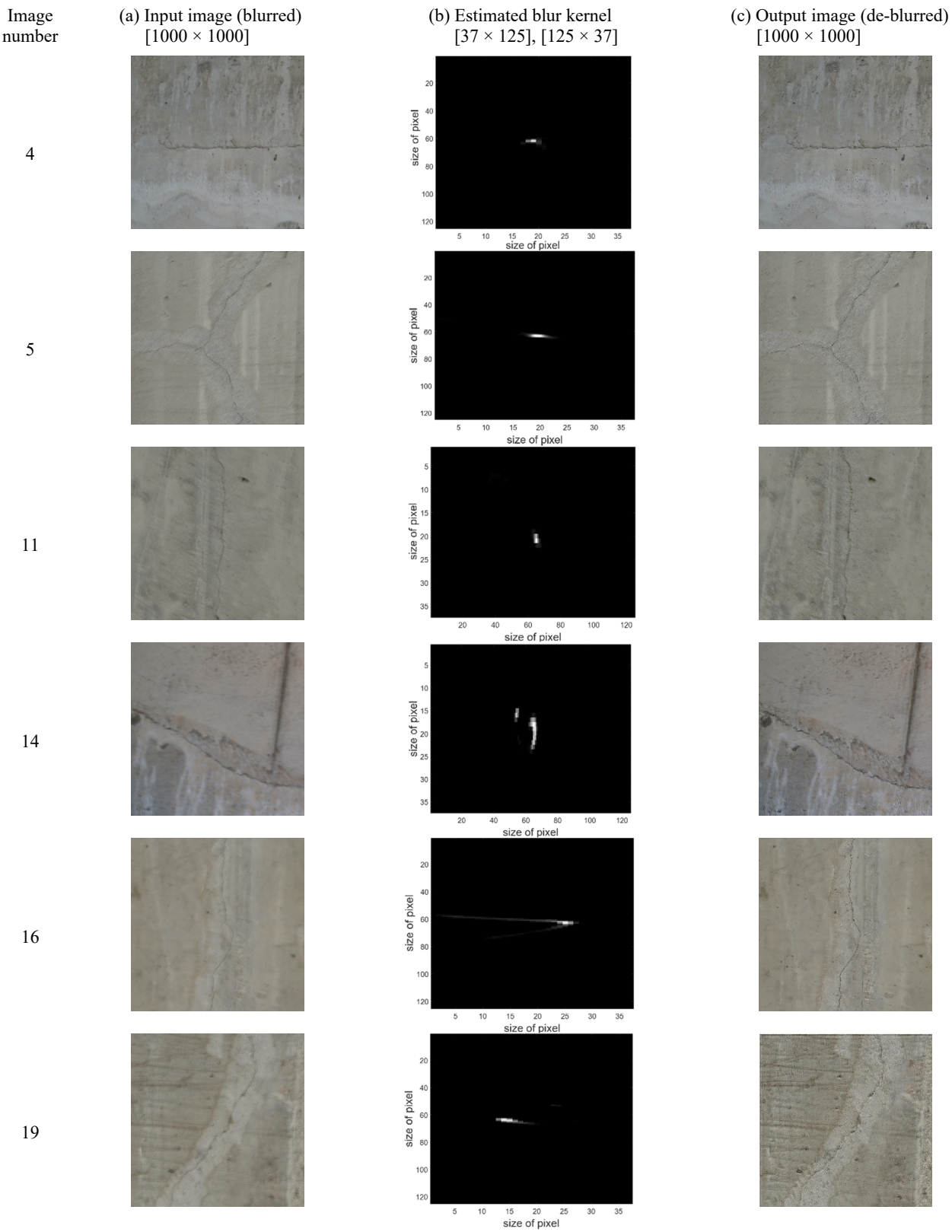

Fig. 15 The results of image enhancement for material images classified as low quality (applied to blurred patches containing damage such as cracks and efflorescence

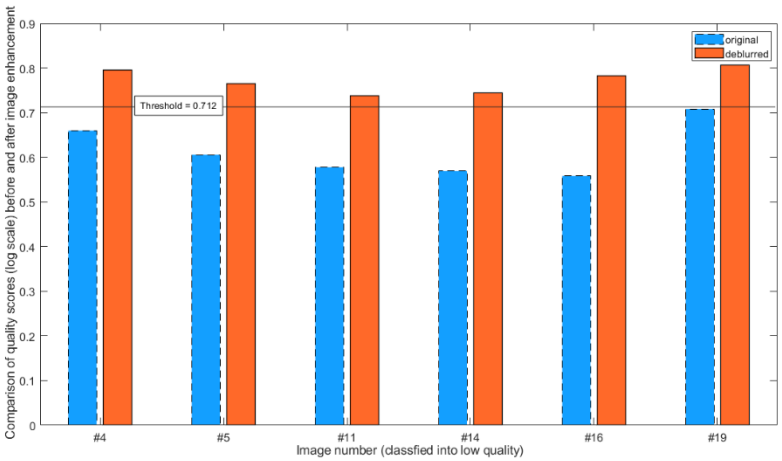

Fig. 16 Comparison of quality scores before and after image enhancement using the proposed method

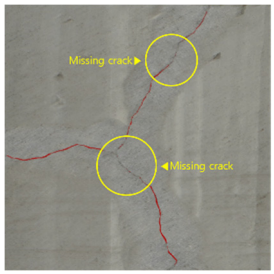

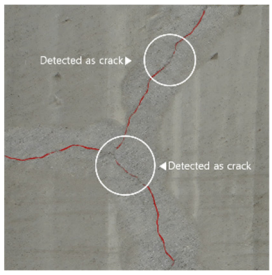

(a) #5 blurred (left) and enhanced (right)

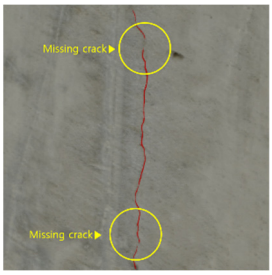

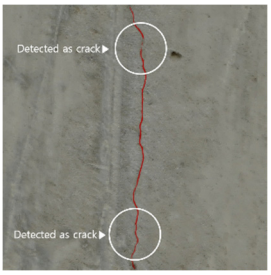

(b) #11 blurred (left) and enhanced (right)

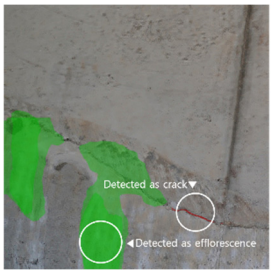

(c) #14 blurred (left) and enhanced (right)

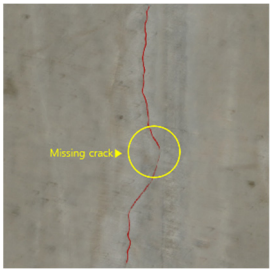

(d) #16 blurred (left) and enhanced (right)

Fig. 17 Damage detection results based on deep learning (Mask R-CNN) for validation of image quality enhancement

Fig. 17 shows the results of damage detection using the Mask R-CNN model. Original images and enhanced images were used as input images, and the effect of performing image quality assessment on the damage detection phase was investigated by comparing the two results. In general, the shape of the crack detected in the blurred image was often missing detection due to discontinuity in the direction of crack propagation as shown in Fig. 18. However, it was confirmed that some information of pixels distorted by blur was restored through blind image deconvolution, and crack detection through deep learning was properly performed as shown in Fig. 18. As shown in Fig. 17(c), not only cracks occurred on the concrete surface but also the detection patterns of efflorescence were partially different, and it was confirmed that cracks that were not detected in the original image could also be detected in the enhanced image.

In order to quantitatively compare the detected damage results using the Mask R-CNN model, crack segmentation was performed. The regions detected as cracks were separately extracted from the blurred image and the enhanced image, and the number of corresponding pixels was compared and shown in Table 5 below. As shown in Fig. 18, in the enhanced image, some cracks not detected in the blurred image were detected due to the discontinuity of cracks caused by blur, and the effective pixel detection rate increased by an average of 41%.

So far, it has been demonstrated that the proposed quality assessment and enhancement method were validated to address the quality issue of UAV images during the bridge inspection. By using the actual UAV image of bridge inspection as a validation set, classification by using the proposed quality metric and process of quality enhancement for low-quality data were performed. Quantitative assessment of the image quality of the material image set was successfully performed, and the improved quality was quantitatively re-measured to confirm the performance of the image enhancement processes.

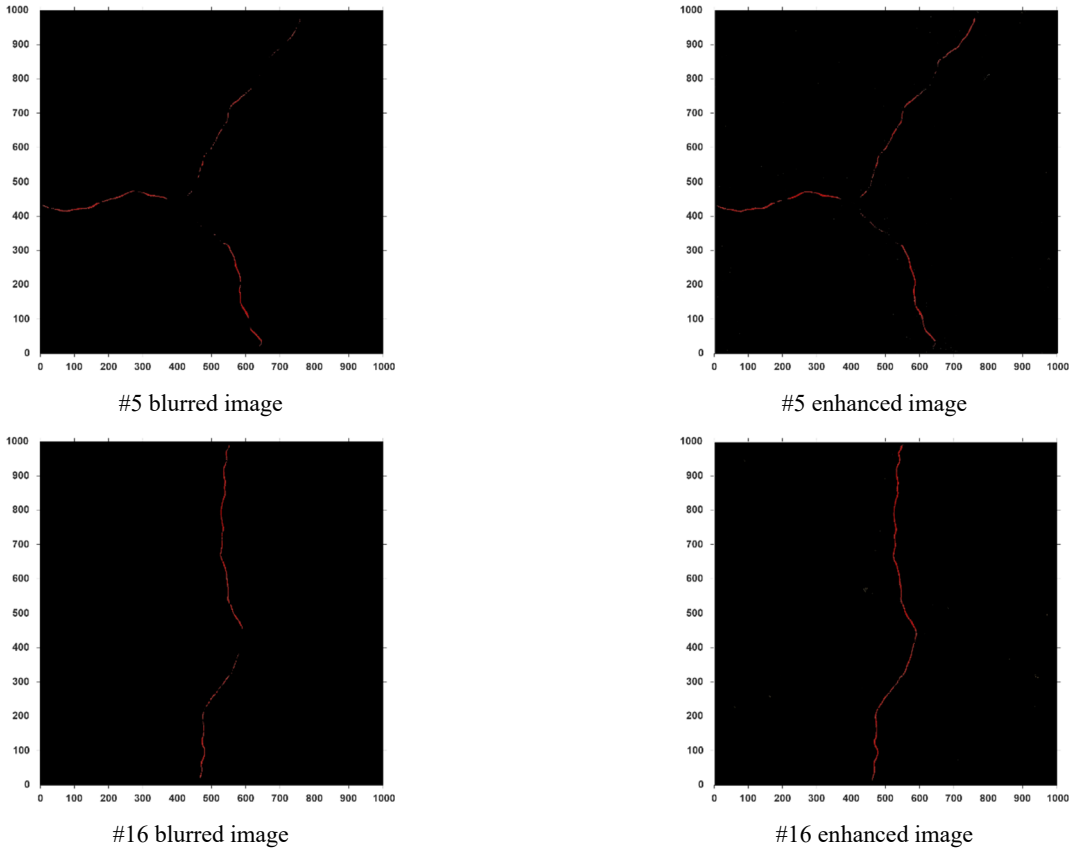

#5 blurred image #5 enhanced image

#16 blurred image #16 enhanced image

Fig. 18 The results of crack segmentation in each image using mask R-CNN model

Table 5 Comparison of damage detection rates before and after quality enhancement

Target images	Number of pixels detected through deep learning		Increase of detection rate
	Blurred image	Enhanced image	
#5	2929	4303	46.91%
#11	2673	3912	46.35%
#16	3515	4611	31.18%

5. Conclusions

It is well known that aerial images acquired during the inspection could be degraded in quality due to various environmental factors. Among them, the most frequently occurring form of quality deterioration in UAV images is motion blur caused by the movement of a camera or a UAV. In this study, a new methodology to address the image quality problem that is mainly encountered in the field of actual bridge inspection using a UAV was developed. Prior to proposing the methodology, the images used in this study were acquired via UAV in a real-world environment, not on a controlled laboratory scale. A new quality metric based on local blur map that can be applied to various and numerous raw images that can be acquired in bridge inspection using UAV was proposed.

In order to verify the proposed method, a comparison with the existing quality metrics was performed, and the result of the proposed metric showed the highest similarity to the classification result by human perception. Thus, it was confirmed that the performance of the proposed method was superior to other metrics. In addition, the deblurring algorithm was applied to mitigate the effect of blur for low-quality images. In this study, a kernel estimation method based on Dirichlet distribution was used in consideration of the non-uniform shape of the blur caused by UAV or camera motion. As a result of performing the quality enhancement, it was confirmed that the degree of blurring decreased by 26% on average, and the damage detection results using the deep learning model (i.e., Mask R-CNN, ResNext-101) also showed that the shape of the crack was preserved and detected in the enhanced image.

The new image quality evaluating and enhancing methodology proposed in this study has the advantage that it can be directly applied to the field of bridge inspection because it has been verified through real-world data. It can also be distinguished from other previous studies in that it can drastically reduce the time and cost required in the image selection and classification process. Therefore, from the perspective mentioned above, the proposed methodology is expected to contribute greatly to the efficiency improvement of the UAV in the field of bridge inspection.

Acknowledgments

This research was financially funded by Construction Technology Research Program funded by Ministry of Land, Infrastructure and Transport (MOLIT) of Korean

government (grant number 19SCIP-C116873-04). This work is also financially supported by Korea Ministry of Land, Infrastructure and Transport (MOLIT) as 「Innovative Talent Education Program for Smart City」.

References

Burdziakowski, P. (2020), "A novel method for the deblurring of photogrammetric images using conditional generative adversarial networks", *Remote Sensing*, **12**(16), 2586. https://doi.org/10.3390/rs12162586

Cho, S. and Lee, S. (2009), "Fast motion deblurring", ACM SIGGRAPH Asia 2009 papers, pp. 1-8. https://doi.org/10.1145/1661412.1618491

Cunningham, C.S., Ransom, D., Wilkes, J., Bishop, J. and White, B. (2015), "Mechanical Design Features of a Small Gas Turbine for Power Generation in Unmanned Aerial Vehicles", *Proceedings of Turbo Expo*: *Power for Land*, *Sea*, *and Air*, 56796, V008T23A021.

Dong, C., Loy, C.C. and Tang, X. (2016), "Accelerating the super-resolution convolutional neural network", *Proceedings of European Conference on Computer Vision*, pp. 391-407.

Dorafshan, S., Maguire, M., Hoffer, N.V. and Coopmans, C. (2017), "Challenges in bridge inspection using small unmanned aerial systems: Results and lessons learned", *Proceedings of the 2017 International Conference on Unmanned Aircraft Systems* (*ICUAS*), pp. 1722-1730.

Duque, L., Seo, J. and Wacker, J. (2018), "Bridge deterioration quantification protocol using UAV", *J. Bridge Eng*., **23**(10), 04018080. https://doi.org/(ASCE)BE.1943-5592.0001289

Gao, J., Liao, W., Nuyttens, D., Lootens, P., Vangeyte, J., Pižurica, A. and Pieters, J.G. (2018), "Fusion of pixel and object-based features for weed mapping using unmanned aerial vehicle imagery", *Int*. *J*. *Appl*. *Earth Observ*. *Geoinform*., **67**, 43-53. https://doi.org/10.1016/j.jag.2017.12.012

Golestaneh, S.A. and Karam, L.J. (2017), "Spatially-varying blur detection based on multiscale fused and sorted transform coefficients of gradient magnitudes", *CVPR 2017*, pp. 596-605.

Hallermann, N. and Morgenthal, G. (2014), "Visual inspection strategies for large bridges using Unmanned Aerial Vehicles (UAV)", *Proceedings of the 7th IABMAS*, *International Conference on Bridge Maintenance*, *Safety and Management*, pp. 661-667.

He, K., Gkioxari, G., Dollár, P. and Girshick, R. (2017), "Mask R-CNN", *Proceedings of the IEEE International Conference on Computer Vision*, pp. 2961-2969.

Jeong, G.Y., Nguyen, T.N., Tran, D.K. and Hoang, T.B.H. (2020), "Applying unmanned aerial vehicle photogrammetry for measuring dimension of structural elements in traditional timber building", *Measurement*, **153**, 107386. https://doi.org/10.1016/j.measurement.2019.107386

Jordan, S., Moore, J., Hovet, S., Box, J., Perry, J., Kirsche, K. and Tse, Z.T.H. (2018), "State-of-the-art technologies for UAV inspections", *IET Radar*, *Sonar & Navigation*, **12**(2), 151-164. https://doi.org/10.1049/iet-rsn.2017.0251

Jung, H.J., Lee, J.H., Yoon, S. and Kim, I.H. (2019), "Bridge inspection and condition assessment using unmanned aerial vehicles (UAVs): major challenges and solutions from a practical perspective", *Smart Struct*. *Syst*., *Int*. *J*., **24**(5), 669-681. https://doi.org/10.12989/sss.2019.24.5.669

Kim, B. and Cho, S. (2019), "Image-based concrete crack assessment using mask and region-based convolutional neural network", *Struct*. *Control Health Monitor*., **26**(8), e2381. https://doi.org/10.1002/stc.2381

Kim, J., Oh, J. and Park, R.H. (2016), "Removing non-uniform camera shake using blind motion deblurring", *Proceedings of the 2016 IEEE International Conference on Consumer Electronics* (*ICCE*), pp. 351-352.

Kim, I.H., Jeon, H., Baek, S.C., Hong, W.H. and Jung, H.J. (2018), "Application of crack identification techniques for an aging concrete bridge inspection using an unmanned aerial vehicle", *Sensors*, **18**(6), 1881. https://doi.org/10.3390/s18061881

Lei, J., Zhang, S., Luo, L., Xiao, J. and Wang, H. (2018), "Super-resolution enhancement of UAV images based on fractional calculus and POCS", *Geo-spatial Inform*. *Sci*., **21**(1), 56-66. https://doi.org/10.1080/10095020.2018.1424409

Liu, L., Liu, B., Huang, H. and Bovik, A.C. (2014a), "No-reference image quality assessment based on spatial and spectral entropies", *Signal Process*.: *Image Commun*., **29**(8), 856-863. https://doi.org/10.1016/j.image.2014.06.006

Liu, Q.F., Xiao, S.F., Huang, K.Z. and Zhong, Z. (2014b), "A SVD-based optical MIMO precoding scheme in indoor visible light communication", *Int*. *J*. *Future Comput*. *Commun*., **3**(6), 421. https://doi.org/10.7763/IJFCC.2014.V3.340

Liu, H., Wang, W., He, Z., Tong, Q., Wang, X., Yu, W. and Lv, M. (2015), "Blind image quality evaluation metrics design for UAV photographic application", *Proceedings of IEEE International Conference on Cyber Technology in Automation*, *Control*, *and Intelligent Systems* (*CYBER*), pp. 293-297.

Liu, Y., Yeoh, J.K. and Chua, D.K. (2020), "Deep learning–based enhancement of motion blurred UAV concrete crack images", *J*. *Comput*. *Civil Eng*., **34**(5), 04020028. https://doi.org/(ASCE)CP.1943-5487.0000907

Mittal, A., Moorthy, A.K. and Bovik, A.C. (2012a), "No-reference image quality assessment in the spatial domain", *IEEE Transactions on Image Processing*, **21**(12), 4695-4708. https://doi.org/ 10.1109/TIP.2012.2214050

Mittal, A., Soundararajan, R. and Bovik, A.C. (2012b), "Making a "completely blind" image quality analyzer", *IEEE Signal Processing Letters*, **20**(3), 209-212. https://doi.org/ 10.1109/LSP.2012.2227726

Morgenthal, G. and Hallermann, N. (2014), "Quality assessment of unmanned aerial vehicle (UAV) based visual inspection of structures", *Adv*. *Struct*. *Eng*., **17**(3), 289-302. https://doi.org/10.1260/1369-4332.17.3.289

Morgenthal, G., Hallermann, N., Kersten, J., Taraben, J., Debus, P., Helmrich, M. and Rodehorst, V. (2019), "Framework for automated UAS-based structural condition assessment of bridges", *Automat*. *Constr*., **97**, 77-95. https://doi.org/10.1016/j.autcon.2018.10.006

Myeong, W. and Myung, H. (2018), "Development of a wall-climbing drone capable of vertical soft landing using a tilt-rotor mechanism", *IEEE Access*, **7**, 4868-4879. https://doi.org/10.1109/ACCESS.2018.2889686

O'Connor, J., Smith, M.J. and James, M.R. (2017), "Cameras and settings for aerial surveys in the geosciences: Optimising image data", *Progress Phys*. *Geography*, **41**(3), 325-344. https://doi.org/10.1177/0309133317703092

Salaan, C.J.O., Okada, Y., Mizutani, S., Ishii, T., Koura, K., Ohno, K. and Tadokoro, S. (2018), "Close visual bridge inspection using a UAV with a passive rotating spherical shell", *J. Field Robot*., **35**(6), 850-867. https://doi.org/10.1002/rob.21781

Seo, J., Duque, L. and Wacker, J. (2018), "Drone-enabled bridge inspection methodology and application", *Automat*. *Constr*., **94**, 112-126. https://doi.org/10.1016/j.autcon.2018. 06.006

Sieberth, T., Wackrow, R. and Chandler, J.H. (2015), "UAV image blur - its influence and ways to correct it", *The International Archives of Photogrammetry*, *Remote Sensing and Spatial Information Sciences*, **40**(1), 33. https://doi.org/10.5194/isprsarchives-XL-1-W4-33-2015

Sieberth, T., Wackrow, R. and Chandler, J.H. (2016), "Automatic detection of blurred images in UAV image sets", *ISPRS J*.

Photogrammetry Remote Sens., **122**, 1-16. https://doi.org/10.1016/j.isprsjprs.2016.09.010

Su, B., Lu, S. and Tan, C.L. (2011), "Blurred image region detection and classification", *Proceedings of the 19th ACM International Conference on Multimedia*, pp. 1397-1400.

Tomiczek, A.P., Bridge, J.A., Ifju, P.G., Whitley, T.J., Tripp, C.S., Ortega, A.E. and Gonzalez, S.A. (2018), "Small unmanned aerial vehicle (sUAV) inspections in GPS denied area beneath bridges", *Proceedings of the Structures Congress 2018*: *Bridges*, *Transportation Structures*, *and Nonbuilding Structures*, pp. 205-216.

Wang, R., Ma, G., Qin, Q., Shi, Q. and Huang, J. (2018), "Blind UAV images deblurring based on discriminative networks", *Sensors*, **18**(9), 2874. https://doi.org/10.3390/s18092874

Xie, S., Girshick, R., Dollár, P., Tu, Z. and He, K. (2017), "Aggregated residual transformations for deep neural networks", *Proceedings of the IEEE Conference on Computer Vision and Pattern Recognition*, pp. 1492-1500.

Yoon, S., Gwon, G.H., Lee, J.H. and Jung, H.J. (2020), "Three-dimensional image coordinate-based missing region of interest area detection and damage localization for bridge visual inspection using unmanned aerial vehicles", *Struct. Health Monitor*., 1475921720918675. https://doi.org/10.1177/1475921720918675

Zhou, X., Mateos, J., Zhou, F., Molina, R. and Katsaggelos, A.K. (2015), "Variational Dirichlet blur kernel estimation", *IEEE Transact*. *Image Process*., **24**(12), 5127-5139. https://doi.org/10.1109/TIP.2015.2478407